Wind-driven stratification patterns and dissolved oxygen depletion in the area off the Changjiang (Yangtze) Estuary

Taavi Liblik[1,2], Yijing Wu[1], Daidu Fan[1,3]

[1] State Key Laboratory of Marine Geology, Tongji University, Shanghai, 200092, China
[2] Department of Marine Systems, Tallinn University of Technology, Tallinn, 12618, Estonia
[3] Laboratory of Marine Geology, Qingdao National Laboratory for Marine Science and Technology, 387P+WW Shinan, Qingdao, Shandong, China

Correspondence to: Daidu Fan (ddfan@tongji.edu.cn)

Abstract. The area off the Changjiang Estuary is under strong impact of fresh water and anthropogenic nutrient load from the Changjiang River. The seasonal hypoxia in the area has variable location and range, but the decadal trend reveals expansion and intensification of the dissolved oxygen (DO) depletion.

Two oceanographic cruises, conducted in summer 2015 and 2017, revealed very different stratification and DO conditions in the area. Strongly inclined oxycline well correlated with the thermocline in both years. Southerly wind caused reversal of the Chinese Coastal Current and as a result, spreading of the CDW (Changjiang Diluted Water) caused pronounced hypoxic zone in the area east and northeast of the river mouth in 2017. Hypoxic layer started right below the CDW layer at 5-8 m depth and extended down to bottom. Strong DO depletion was also observed in the shallow coastal slope in the southern part of the study area. High DO utilization there closely coincided with the interaction zone of the upwelling and fresher surface water. The stratification and hypoxia pattern observed in the area in 2017 is prevailing phenomena during summers if considering the long-term wind statistics.

Northeasterly winds supported southward transport of the CDW before the survey in 2015. Consequently, low DO was found in the southern part of the study area while subsurface layer in the northern part was ventilated. Weaker than long-term average summer monsoon is required for the existence of such pattern.

Importance of the wind forcing was confirmed by remotely sensed sea surface salinity fields and by circulation simulation. We suggest wind forcing, together with river run-off are likely main contributors of determining the synoptic, seasonal and inter-annual time scale variations of the extent and location of low DO areas off the Changjiang Estuary.

1   Introduction

Dead zones in the coastal ocean have spread since the 1960s (Diaz and Rosenberg, 2008). Besides eutrophication (Diaz and Rosenberg, 2008), climate change (Altieri and Gedan, 2015) intensifies DO depletion. Estuaries and other regions of fresh water influence are typically very productive regions and often experience hypoxia (Conley et al., 2009; Cui et al., 2019; Obenour et al., 2013; Testa and Kemp, 2014). Natural and anthropogenic nutrient load in these areas leads to intensive sedimentation of organic matter. DO is used by concurrent decomposition of detritus by bacteria in the sub-surface layer. If the decline of DO exceeds DO import or production, the DO concentrations decrease. Deep layers below euphotic zone can receive DO by physical processes only – lateral advection and vertical mixing.

Hypoxia is natural phenomena off the Changjiang Estuary, as evidences of its existence extend back to 2600 years at least (Ren et al., 2019). However, hypoxic area has been expanded in recent decades (Chen et al., 2017; Ning et al., 2011; Zhu et al., 2011), which can be mostly related to the eutrophication (Wang et al., 2016). A low DO zone off the estuary can be found from spring (Zuo et al., 2019) until decay of stratification in autumn (Wang et al., 2012). The formation and maintenance of seasonal hypoxia has been related to various physical, biogeochemical and biological processes (Ning et al., 2011). Hypoxia off the Changjiang Estuary is in literature often divided to the southern and northern areas (Wei et al., 2017a; Zhu et al., 2011). The northern part features shallow (20 – 40 m) and flat sea bottom while the southern part characterize a deep trough with water depth > 60 m and steep slope. Numerous small peninsulas and islands occupy in the southern part with irregular coastline.

The area is intensely impacted by huge river discharge from the Changjiang (Beardsley et al., 1985; Xu et al., 2018). Nutrient rich freshwater mixes with ocean water to form the Changjiang Diluted Water (CDW). Enhanced primary production in the CDW causes intense detritus accumulation and DO consumption in the near-bottom layers (Chen et al., 2017; Wang et al., 2017, 2016; Zhou et al., 2019). The CDW is separated from the deeper water with a shallow halocline, which often coincides with the seasonal thermocline (Zhu et al., 2016). The shallow pycnocline impedes vertical mixing and vertical DO transport downwards. Thus, the presence of the CDW provides favorable conditions for hypoxia formation in the layer below pycnocline. Moreover, the shallow pycnocline supports accelerated warming in summer (Moon et al., 2019) and as consequence pycnocline strengthens even more. Shallower areas near the river mouth are strongly impacted by tidal forcing (Li et al., 2018). However, in the open sea the contribution of tides in the vertical mixing budget is low comparing to the wind stirring (Ni et al., 2016). Abrupt wind mixing events can weaken stratification and considerably increase DO concentrations in the deep layer (Ni et al., 2016). However, such vertical mixing also cause nutrient flux to the upper layer (Hung et al., 2013) and as a result primary production in the upper layer and DO consumption in the deep layer is enhanced (Ni et al., 2016).

Circulation and hydrography near the Changjiang Estuary are besides the CDW impacted by the Taiwan Warm Current (TWC) and its northward extension, Chinese Coastal Current (CCC), and Kuroshio intrusions (Lie and Cho, 2002, 2016; Zhang et al., 2007). Geostrophic currents in the area are modified by wind forcing, which exhibits seasonal alternation of winter and summer monsoons (Lie and Cho, 2002). Winds from north and northeast prevail during the winter monsoon and southerly winds dominate during the summer monsoon (Chu et al., 2005). Summer monsoon favors upwelling formation in the Eastern China Sea (ECS) (Hu and Wang, 2016), including sea areas nearby the Changjiang Estuary (Xu et al., 2017; Yang et al., 2019). Upwelling events bring large amounts of

85   nutrients to the surface layer (Wang and Wang, 2007), which cause increase of primary production and decrease of DO concentrations in the near-bottom layer (Chen et al., 2004; Zhou et al., 2019).

Recent modeling study (Zhang et al., 2018) has demonstrated that the CDW is very mobile and as a result location and areal extent of bottom hypoxia is variable as well. Thus, distributions of oceanographic fields mapped during an occasional research cruise could depend on simultaneous synoptic scale forcing conditions and does not

90   necessarily represent the hydrophysical and chemical situation in particular summer. In order to put oceanographic cruise results to more general context, observed ocean variables must be linked to the forcing.

Hypothesis of the present study is that prevailing physical factors, wind forcing and river run-off mainly determine the stratification patterns and as consequence the location and areal extent of the DO depletion off the Changjiang Estuary. This means that changes in forcing over various time scales (synoptic, inter-annual, decadal) cause also

95   changes in the patterns (e.g., the stratification or the location of the hypoxic area). To testify this hypothesis, we (1) described the observed patterns (horizontal and vertical distributions) of stratification and DO off the Changjiang Estuary during the two cruises, (2) explored the potential link between physical variables and DO distributions, and (3) investigated the forcing mechanism behind observed patterns.

Following a description of the measurements and the methods used, this paper presents an analysis of (1) spatial

100   distributions of temperature, salinity, DO and derived variables, (2) temporal changes and forcing behind the observed distributions. Finally, the analysis of our results are discussed and concluded.

105

2 Data and Methods

We have performed two surveys in the Changjiang Estuary and the adjacent sea on board the RV Zheyuke-1 from 27 August to 5 September in 2015 and from 24 to 29 July in 2017, respectively. CTD (Conductivity, Temperature,

110   Depth) and DO profiles were obtained from 110 stations in 2015 and 83 stations in 2017, but not all the stations were included in the present study. Layout of the stations used in the present work is shown in Fig 1. At all stations vertical profiles of temperature, salinity and DO were recorded with the SBE 25plus Sealogger CTD with DO sensor SBE43. The DO sensor was calibrated against water sample analyses conducted by Winkler titration method. Linear regression between sensor and sample DO data for the 2015 and 2017 was found respectively: *DO*

115   *= $DO_{SBE} \times 0.98 – 0.09$ ($r^2 = 0.93$ n = 191) and $DO = DO_{SBE} \times 0.98 – 0.06$ ($r^2 = 0.99$ n = 98)*, where DO_{SBE} is the DO recorded by SBE43 sensor (Wu et al., 2019).

Salinity data in the present work is presented in the Practical Salinity Scale (Fofonoff and Millard Jr, 1983) and density as potential density anomaly (σ_0) to reference pressure of 0 dbar.

8-day running average Sea Surface Salinity (SSS) calculated from Soil Moisture Active Passive (SMAP) mission

120   (Meissner et al., 2018) was used for the spatial extent estimation of the CDW from 2015 to 2018. Remotely sensed salinity well agreed with the in-situ salinity measurements (Fig. 2) at the mooring station M1 (Fig. 1).

Reprocessed 6 hourly wind observations with horizontal grid size of 0.25° from 1993 to 2018 downloaded from Copernicus Marine Service (product ID WIND_GLO_WIND_L4_REP_OBSERVATIONS_012_006) was used to describe wind conditions. Wind stress was calculated following Large and Pond, (1981):

125 $\tau = \rho_{air} \, C_D \, IUIU_{10}$, (1)

where C_D is the drag coefficient and U_{10} is the wind speed at the reference height of 10 m.

Current speed and direction from the Copernicus Marine Service reanalysis product GLORYS12V1 from 1993 to 2018 was downloaded. The global eddy resolving model has regular horizontal grid with step of approximately 8 km (1/12°) and standard vertical levels with resolution increasing from 1 m near the surface to 8 m around 50 m

130 depth and 17 m around 100 m depth. Remotely sensed and in-situ observed temperature, salinity, and sea level were assimilated to the model. The model has too rough resolution to estimate details of meso- and finer-scale features in the area. However, it can be used to estimate the general current patterns. Simulated current field reasonably well reproduced the observed spreading direction of the CDW.

Depending on marine organisms, hypoxia can have various definitions (Vaquer-Sunyer and Duarte, 2008). In the

135 preset study, hypoxia was defined as DO concentration of <3.0 mg l⁻¹. The apparent DO utilization (AOU) is the difference between DO concentration at the saturation level and measured DO concentration in water with the same temperature and salinity and is calculated as follows

$AOU = DO_s - DO_M$; (2)

where DO_S is DO concentration at the saturation level (Weiss, 1970) and DO_M is the measured DO concentration.

140 Total AOU (g m⁻²) in the water column was calculated as

$$AOU_{TOT} = \sum_{z=0}^{z=h} \begin{array}{l} 0, if \, AOU \leq 0 \\ AOU(z)dz, if \, AOU > 0 \end{array}$$ (3)

where $AOU(z)$ is the AOU profile and h is the water column depth.

Daily (2015 and 2017 summer) and monthly (2001-2018) river discharge data from Datong hydrological station (see location in (Xu et al., 2018) were used in analysis.

145 Remotely sensed salinity data are linearly interpolated from four closest grid points to the location of measurements.

3 Results

150 ### 3.1. Spatial patterns

In the following we analyze temperature, salinity, stratification and DO distribution patterns observed in summers 2015 and 2017.

The water of SSS < 30 psu was observed along the coastal zone of the entire study area in 2015 (Fig. 3). The

155 isohaline 25 psu reached to 29.3° N in the southern part of the study area while its northern boundary was at 31.7° N near the mouth of the Changjiang Estuary in 2015. In 2017 the isohaline 25 psu reached only to 30.6° N in the southern part of the study area. While fresher water than 25 psu was also observed in the east and northeast off the Changjiang Estuary. Thus, the CDW southward spreading has been prevailed before the survey in 2015, but the CDW eastern and northeastern diversion was observed prior to survey in 2017.

160   The surface temperature was generally lower in the study area in 2015 (Fig. 3). The maximum SST in the study area was 28.3 °C (31.3 °C) in 2015 (2017). Colder surface water was observed near Zhoushan Islands and along Zhejiang coast (28.5° N to 31° N), and in the northern part of the study area (>31.5° N) in both years. The SST was much lower in these regions, but colder area covered smaller areas in 2017.

The near-bottom temperature difference between the two surveys was particularly large in the northern part of the

165   study area (Figs. 3-5). Near-bottom temperature was 24-25 °C at 20-30 m sea depth in 2015 while it was 21-22 °C in 2017. Likewise, near-bottom water was saltier in 2017. The location of minimum near-bottom temperature was at 50-60 m sea depth in the southern part of the study area in 2015. The minimum temperature was closer to the coast and at shallower depths in 2017.

Changes of stratification in the study area are described by the difference between the surface and near-bottom

170   layer density (Fig. 6). Relatively weak stratification (< 3 kg m^{-3}) was observed in the northern part of the study area in 2015. Stratification was stronger (>3 kg m^{-3}) in the area south off the Changjiang Estuary, being particularly strong (>6 kg m^{-3}) at 20-30 m sea depth. In this area, the CDW covered the surface layer, and cold and saltier water mass occupied the near-bottom layer. Near the coast and offshore such strong stratification was not observed, i.e., the dense deep layer water did not intrude into the shallower areas and the CDW did not spread further offshore.

175   Strongest stratification (>6 kg m^{-3}) was observed in the northern part of the study area in 2017 (Fig. 6). The areal extent of strongly stratified region fitted with the area of CDW distribution in the surface layer. Stratification was weaker (<3 kg m^{-3}) in the very shallow areas (< 10 m), where cold and saltier water mass did not exist and in the southeastern part of the study area, where the CDW did not spread and bottom water was warmer than at the core of the cold water mass.

180   Low DO concentrations (2-3 mg l^{-1}) in the near-bottom layer occurred at sea depths of 25-60 m in the southern part of the study area in 2015 (Figs. 4, 6). Near-bottom DO concentrations further offshore (east) and in the north were 3-5 mg l^{-1} and higher in shallower depths. Low DO area (2-3 mg l^{-1}) only partly overlapped with the CDW distribution, but fitted well with the area occupied by cold (< 20 °C) water mass in the near-bottom layer. The vertically integrated AOU maximum (>150 g m^2) pattern was observed between 30-31° N and 123-124 ° E in

185   2015.

Two low DO concentration (<3 mg l^{-1}) zones were observed in the near-bottom layer in 2017 (Figs. 5 and 6). The one in the north well overlapped with the low saline CDW and strong stratification area. Hypoxia there started at 5-8 m depth already and was closely linked to the location of the pycnocline. The second low DO concentration zone was observed in shallow depths (10 - 30 m) at the coastal slope in the southern part of the study area

190   overlapped with colder SST and lower SSS (Fig. 5). This indicates that interaction between coastal upwelling, which bring subsurface water to shallower depths (euphotic zone) and fresher surface water created favorable conditions for the DO consumption. The vertically integrated AOU had highest values (>150 g m^2) in the northern part of the study area in 2017.

The low DO concentration zones in the near-bottom layer can be found in various sea depths, e.g., as shallow as

195   10 m in 2017. Strong enough stratification makes DO depletion possible in such a shallow depth. The question is whether the DO depletion is linked to a certain physical property of water. We determined the AOU isoline 2 mg l^{-1} as the upper boundary of the DO depletion, i.e. the oxycline. We found high correlation ($r^2 = 0.81$, p < 10^{-10}, n < 44 in 2015, and $r^2 = 0.98$, p < 10^{-10}, n = 34 in 2017) between isotherm 24.5 °C and AOU isoline 2 mg l^{-1} depth. Thus, the vertical location of the thermocline determined the vertical location of the oxycline. The

200   thermocline/pycnocline provides barrier for vertical mixing and under the cline DO depletion can develop. There
        was an inclination of the both clines in both years (Fig. 7). The inclination was particularly steep in 2017. Both
        isolines were located around 50 m depth in the southeastern corner of the study area while in the shallow areas in
        the west and north the same layer was at 5 – 10 m depth. Such an inclination of isotherms and cold SST near the
        coast is an indicator of upwelling. Deeper colder water intruded along the coastal slope shallower to replace the
205   former upper layer water. The inclination of clines was not that pronounced and it was rather north-south directed
        in 2015. It is noteworthy that the high vertically integrated AOU area overlapped with shallow position of isolines
        in 2015. It means that high total AOU there (comparing to neighboring areas) was related to the thick subsurface
        DO depleted layer and not to the lower (comparing to surrounding area) DO concentrations.
        We have captured two completely distinct situations of stratification and DO distributions in summers 2015 and
210   2017. The differences between the two years are outlined in the Table 1. Prevailing of either pattern in the physical
        fields has consequences to the biogeochemical fields and ecosystem in general in the area. The main questions
        addressed next are: what are the main drivers causing the distinct patterns? What is the quantified forcing behind
        formation of the patterns?

215

220

3.2. Forcing, time-series

225

        The observed discrepancies of general features in the two cruise surveys can be driven by several forcing
        mechanisms. The riverine water is a source of buoyancy flux, causing current to flow south along the coast. Mean
        discharge at Datong hydrological station in the two summers (1 June to 31 August) was rather similar, 44 000 -
        45 000 m^3s^{-1}. We consider the time lag of 1 week for water propagation from Datong to the river mouth (Li and
230   Chen, 2019) in further discussion.
        Comparing two years discharge data in June, discharge was higher in 2015. Contrary in July discharge was higher
        in 2017. Daily discharge maxima peaked at 58 000 m^3s^{-1} on 1 July in 2015 and at 70 000 m^3s^{-1} on 13 July in 2017.
        According to the typical residual current velocities off the estuary (Peng et al., 2017) and along the coastline in the
        south (Wu et al., 2013), it should take a few days to weeks for the water from the river mouth to reach offshore as
235   we registered in 2017 or to Zhejiang coast in the south in 2015. We assume that 7 days accumulated run-off (or
        wind forcing) is enough to alter the field distributions off the estuary. Mean river flow during a week before surveys
        was 30 000 m^3s^{-1} in 2015 and 65 000 m^3s^{-1} in 2017, respectively. The question is how much of riverine water
        remains in the river plume bulge and how much is advected to the neighboring areas. The discharge Rossby number

$R_0 = U/Bf$ (Fong and Geyer, 2002), where U is the river inflow velocity, B is the river mouth width (34 km) and f

240   is the Coriolis parameter (7.5 10^{-5}), describes the share of riverine water in the bulge and downstream current. The estimated R_0 varied between 0.08 and 0.22 in 2015 and 2017. Relatively low R_0 shows that most of the riverine water contributes to the coastal geostrophic current but less to the bulge. Variations in discharge influence the across-shore extent of plume and the width of buoyant current. According to the theory by Lentz and Helfrich (2002) the width of buoyant current would be 70 km in the case of ambient and CDW water density difference of

245   10 kg m^{-3}, coastal slope of 10^{-4} and discharge of 65 000 m^3 s^{-1} before our survey in 2017. The width would be 18 km if the inflow volume of 30 000 m^3 s^{-1} in 2015 was considered. Thus, the variability in the river discharge only somewhat explain the discrepancy between the two surveys, particularly more extensive spreading of the CDW eastward in 2017. However, it does not explain the northeast advection of the CDW that far in 2017. Likewise, it remains unclear why southward transport of the CDW was much more limited in 2017 than 2015. While several

250   indicators hint that wind-driven transport could be behind the discrepancy between the 2015 and 2017 observations, including stronger across shore inclination of the pycnocline, offshore advection of the CDW, and onshore advection of the colder sub-pycnocline water in 2017. Such features were not found during the survey in 2015, but southward advection of the CDW revealed instead. Our hypothesis is that the dominant factor behind the discrepancy of the two surveys is wind forcing.

255   As argued previously, we assume the thermohaline fields in the study area were established by the forcing one week before. Mean wind, surface currents and bottom currents one week prior to the surveys are presented in Fig. 8. The mean airflow was from northeast prior to the 2015 survey and from south prior to the 2017 survey. Northeasterly wind should cause downwelling and accelerate alongshore buoyant current towards the south. This current was clearly detectable in the mean surface current plot in 2015 (Fig. 8c), along the coast from 32.5° N to

260   28° N. Such coastal current did not reveal before the 2017 survey. Weak mean flow towards the east or northeast could be noted near the mouth of the Changjiang River in 2017. Likely, the buoyant coastal current was altered and the CDW was transported across shore by southerly wind forcing. Thus, simulated current patterns and wind forcing prior to the two surveys were qualitatively in accordance with observed salinity fields in the surface layer (Fig. 3). Main difference between the two years in the bottom layer was the stronger northward flow in 2017 (Fig.

265   8). Penetration of the deep layer water to the shallower areas, towards the river mouth occurred in 2017. This coincided with our observations in terms of the stronger inclination of clines and presence of the colder water mass in the northern part of the study area in 2017 (Fig. 3). Because southerly wind forced offshore transport of the surface water, deep layer water intruded to the shallower depths for compensation in 2017. It has to be noted that southward coastal flow was almost negligible (unlike in the surface) in the bottom layer in 2015, showing the

270   baroclinic nature of the current.

In order to verify the sensitivity of the buoyant coastal current to wind forcing, simulated current and wind data from June to September in 1993–2018 were used. First, we calculated daily mean meridional (alongshore) upper layer (0-5 m) current velocity component v_m at the zonal section of 31° N (section S1) from 122.1° to 122.6° E (see red dashed line in Figs. 8c-d). Correlation was calculated between the current velocity component v_m and

275   wind from different directions. The best correlation ($r^2 = 0.76$, $p < 10^{-10}$, n = 3025) was found with the one-day (prior to the modeled current value) mean SE–NW wind velocity component w_c (Fig. 9). Thus, the meridional current along the coast well correlates with wind.

Simulated near-bottom currents (Fig. 8e) suggest that cold and saltier water (comparing to 2015 observation) was advected to the northern part of the study area as compensation flow to the offshore flow in 2017. Moderate winds before the 2017 survey (Fig. 10) could not mix the cold and DO depleted deep layer water into the upper layer. However, stronger wind impulse with speeds up to 11-12 m s^{-1} occurred a few days before the start of the survey in 2015. Upper mixed layer depth created by wind stirring was estimated by the formula describing the turbulent Ekman boundary layer $h = 0.1\ u_*\ /f$ (Csanady, 1981), where $u_* = (\tau/\rho_w)^{1/2}$ is friction velocity, q_w is water density, τ is wind stress and f is Coriolis parameter. Vertical mixing reached down to 15-16 m depth according to this empirical method before the 2015 survey. Note that our estimation is based on 6-h average wind speed and stronger winds, which probably cause deeper mixing to occur in shorter time scales. Thus, wind stirring could considerably weaken the stratification before the 2015 survey, as evident by the presence of warmer, fresher water with higher DO concentration in the deep layer. Since the wind was from the northeast before the survey (Fig. 8), downwelling can be responsible for this weaker stratification as well.

Further we analyzed time-series of wind speed, SE-NW wind stress component (τ_c), meridional current velocity component (v_m) at the section S1, and the Changjiang river run-off in June-September 2015 and 2017 (Fig. 10). Wind stress $\tau_c > 0$ and northward current component prevailed from June to early August in 2017. Larger wind stress events alternated with calmer periods from June to late August in 2015. During the periods of low $\tau_c > 0$, current was often directed southward. The $v_m < 0$ occurred more frequently in June-July 2015 compared to the same period in 2017. Latter is reflected in monthly salinity distributions. We defined the CDW as salinity of < 30 psu and calculated its spatial monthly occurrence from June to September in 2015-2018 using satellite surface salinity distributions (Fig. 11). Lowest areal extent of the CDW was observed in September in both years, 2015 and 2017. The CDW mainly advected to the northeast and east in all summer months in 2017. Northeastward transport of the CDW could be noted also in 2015, but the CDW occupied areas in the southern part of the study area as well. We can conclude that our survey in 2017 well described the prevailing situation of the CDW spreading in summer 2017. In summer 2015, we captured the situation, where the CDW spread to the south, but during summer northeastward spreading occurred as well.

Next we make an attempt to quantify the two CDW spreading cases caused by wind forcing through analyzing model simulation and wind data from the period June–September in 1993-2018. We averaged the simulated v_m to different wind velocity component classes with step of 0.25 ms^{-1} and found that if the $w_c = 0$ m s^{-1}, current velocity component v_m would be on average -13 cm s^{-1} (i.e., southward) at S1. We can assume that this is the mean geostrophic component of the current velocity. Daily mean wind velocity component w_c of 5.6 m s^{-1} is required to reverse the current and have the same magnitude at S1 (v_m = +13 cm s^{-1}). This corresponds roughly to the wind stress τ_c of 0.04 N m^{-2}. Wind stress τ_c of 0.02 N m^{-2} corresponds to the v_m of 0 cm s^{-1}, i.e., coastal current is altered.

We analyzed the simulated current data in June–September from 1993 to 2018 and averaged the cases, when daily mean wind stress component τ_c was < 0 and ≥ 0.02 N m^{-2} (Fig. 12). The same circulation features, but more pronounced, stand out as before the surveys in 2015 and 2017 (Fig. 8). In the case of $\tau_c < 0$ N m^{-2} southerly flow prevailed in the surface layer along the coast and the mean currents in the near-bottom layer were rather weak. In the case of $\tau_c \geq 0.02$ N m^{-2} flow was northward along the coast, and shifted north or towards the river mouth in the deep layer.

320

Discussion

Two distinct stratification and DO distribution patterns were observed in the area off the Changjiang Estuary in
325   the summers of 2015 and 2017. There was a stronger DO depletion in the southern part of the study area, off
Zhejiang coast in August-September 2015, while intense hypoxia was observed in the northern part of the study
area in July 2017. Likewise, remarkable DO depletion was observed in the southern part at the upwelling zone in
2017. Similar hypoxia patterns in August (our July 2017 observations) and October (our August-September 2015
observations) were observed in 2006 (Zhu et al., 2011). As we have argued, the main reasons for the different
330   hypoxia patterns are variations in the wind forcing and river discharge. Summer monsoon and higher discharge
both favor across-shore transport of CDW and development of hypoxia in the northern part of the study area. Both,
maximum frequency of southerly wind and river discharge in the annual cycle occur in July-August (Fig. 13). In
accordance with the annual cycle of wind, highest frequency of upwelling events occurred in July-August as well
(Xu et al., 2017). Wang et al. (2012) explained the annual cycle of the location of near-bottom DO minimum by
335   seasonal change of stratification due to river discharge and warming/cooling of the upper layer. We suggest that
the southern location of the DO minimum in June and September, and the northern location, as observed in July-
August 2006 (Fig. 3 in Wang et al. (2012) paper), are related also to the seasonality of wind forcing and respective
Ekman transport.

In figure 11 we presented monthly occurrence of CDW (as salinity < 30) from June to September 2015-2018. One
340   can see how year 2015 distinguishes with low value in the inter-annual time-series of wind stress of $\tau_c \geq 0.02$ N
m^{-2} (Fig. 13) and with considerable southward advection of the CDW (Fig. 11). This well demonstrates that wind
regime plays an important role in the inter-annual variations of the hypoxic area location (Fig. 6). Year 2016 stands
out in terms of wind forcing close to inter-annual mean, but with very high river discharge (Fig. 13). One can see
that offshore advection prevailed in 2016 (Fig. 11). This indicates that if wind forcing is close to long-term average
345   hypoxia more likely will occur rather in the east of the river mouth (northern part of study area) and hypoxia
occurrence in the south is more limited. In other words, hypoxia in the southern part (as we observed in 2015)
occurs if the summer monsoon is considerably weaker than long-term mean. Indeed, hypoxia in the south has been
quite rare in 1998 – 2013 (Chen et al., 2017). As a consequence of large river runoff clearly largest CDW spreading
area occurred in year 2016 out of the four years (Fig. 11). Occurrence of wind stress $\tau_c \geq 0.02$ N m^{-2} was higher
350   than average and river discharge was lower than average in 2018 (Fig. 13) and this reflected well in the CDW
distribution (Fig. 11). One can see that CDW covered smallest area out of four years and prevailing transport
direction was towards the north or northeast. Correlation between the CDW plume area and river discharge has
been suggested by Kang et al. (2013). From our stratification and DO distribution observations and their
dependence on wind forcing, and CDW spreading direction and extent (Fig. 11), DO depleted area should have
355   occurred in the northern part both in 2016 and 2018, with larger extent than in the former year.

We estimated that wind stress of $\tau_c \geq 0.02$ N m^{-2} is necessary to alter the geostrophic coastal current and create favorable conditions for hypoxia in the northern part. Compared with inter-annual mean (1992 - 2018) in same months, the occurrence of $\tau_c \geq 0.02$ N m^{-2} in June – September in 2015 and 2017 was relatively lower (Fig. 13). The same applies to the comparison of the months July-August. River discharge in June – September was close to the inter-annual mean (2001 - 2018) in both years. Slightly lower (higher) discharge than average occurred in 2015 (2017) if only the months July-August were taken into account. Inter-annual variations of occurrence of wind stress $\tau_c \geq 0.02$ N m^{-2} in July-August are quite large (Fig. 13). When the occurrence of $\tau_c \geq 0.02$ N m^{-2} was $\geq 50\%$ in the summers of 1995, 2012, 2013, and 2018; stratification and DO patterns probably occurred as coastal upwelling-related hypoxia in the south and large hypoxic area in the north as we observed in 2017 (Fig. 6). Large hypoxic area in the north has been documented for instance in August 2013 (Ye et al., 2016). Contrary, in summers when the occurrence of $\tau_c \geq 0.02$ N m^{-2} was less than inter-annual mean (1992, 1993, 1996, 1998, 1999, 2002, 2007-2009, 2014), hypoxia was also expected to have occurred in the southern part as we observed in 2015. Such situation has been captured for instance in 1998 (Wang and Wang, 2007).

The estimated discharge Rossby number indicated that most of the river discharge contributes to the downstream geostrophic current. It well agrees with earlier estimates that about 80-90% of the discharge accounts to freshwater transport of coastal current (Li and Rong, 2012; Wu et al., 2013). This means that most of the river discharge does not remain in the river plume bulge, but impacts the surrounding areas off the estuary. Applying linear regression analysis between wind and modeled current velocity we estimated the southward geostrophic component of the current velocity to be on average 13 cm s^{-1} at section S1. The southward coastal current was measured in winter by Wu et al. (2013). They estimated the maximum detided current speed up to 50 cm s^{-1}, but it included also wind-driven component, which in winter supports flow to the south (Wu et al., 2013).

Offshore, east- or northeastward advected CDW, as we observed in 2017, might form detached eddies due to interaction of the Ekman flow and density driven frontal currents (Xuan et al., 2012). Physical and chemical characteristics of eddies can differ significantly from the surrounding water much further from our study area (Wei et al., 2017).

Offshore transported CDW occurred simultaneously with coastal upwelling in 2017, as both processes require southerly wind. Shoreward, upslope penetration of the sub-thermocline water and hypoxia in the upwelling – CDW interaction zone were observed. Upwelling, induced by southerly winds and its relaxation supported by northerly winds was captured by cross-sectional in-situ measurements by Yang et al. (2019). Idealized numerical experiment by Liu and Gan (2014) showed that southeasterly wind forcing caused the development of upwelling and shoreward intrusion of colder water in the study area. Wei et al., (2017) showed how the coupling of the CDW plume front and upwelling caused DO minimum at the sloping bottom. Likewise N/P ratio and primary production in the CDW is considerably modified by upwelling (Tseng et al., 2014). Phosphate transport by upwelling reduces phosphorus deficiency in the CDW water and therefore promote phytoplankton growth and nitrate uptake (Chen et al., 2004; Zhou et al., 2019).

Time-series of wind displayed large variations in wind forcing in shorter time scales (days to weeks) (Fig. 10) which may alter the stratification pattern and DO distributions considerably. Numerical simulation by Zhang et al. (2018) showed that wind-induced redistribution of Changjiang river bloom changes near-bottom DO conditions rapidly. Also, it has been shown that vertical mixing caused considerable variations in DO concentrations in the near-bottom layer (Ni et al., 2016). In July 2015, 1.5 month before our survey, hypoxia was destroyed by typhoon,

but two days later hypoxic conditions were re-established (Guo et al., 2019). Our field measurements showed that oxycline is strongly linked to the thermocline (Fig. 7). Besides enhanced (or impeded) vertical diapycnal mixing, DO conditions can be altered by vertical movement of isopycnals. Ni et al. (2016) published valuable dataset of the time-series in the near-bottom layer. They linked the increase of DO concentrations in the near-bottom layer

400 with the vertical mixing and DO decline in the near-bottom layer with the primary production and consequent decomposition of detritus. One can see several cases from their time-series (Fig. 2 in Ni et al. (2016)), when near-bottom temperature drops. Those events must be related to the advection of colder water and uplift of the thermocline. At the same time, DO declined during those events. Penetration of the cold, low DO water upwards along the coastal slope appear as temperature and DO decline in the point measurement time-series. On the other

405 hand there were some events, where near-bottom layer temperature rises, but sea surface temperature does not change much (e.g. in the beginning of their time-series, fig. 2 in Ni et al. (2016). In these cases DO concentrations increased in the near-bottom layer. Such events can be associated rather to the downward movement of the thermocline or advection of warmer water than vertical mixing. Thus, vertical location and movement of the thermocline has important role in the near-bottom DO distributions at coastal slope. Pycnocline dynamics,

410 including downwelling studies, as suggested by Hu and Wang, (2016), are important to investigate in future. Those studies are difficult to arrange with conventional research vessel surveys only. Autonomous measurement platforms, such are profiling moorings (Lips et al., 2016; Sun et al., 2016), moored sensor chains (Bailey et al., 2019; Venkatesan et al., 2016), which allow capturing the variability in necessary vertical- temporal resolution can be used. Underwater gliders (Liblik et al., 2016; Rudnick, 2016) might be complicated to use due to strong

415 tidal velocities and heavy ship traffic, but are worthy to consider as well.

Our observations indicated that two physical conditions in the water column must be present for the development of hypoxia. First, high AOU occurred only below thermocline. Secondly, the fresher CDW was present in the surface layer when the areas of hypoxic bottoms were observed (Figs. 4-5). Interestingly, these two conditions for hypoxia were valid in very different situations. Shallow (4-6 m) and sharp thermocline coincided with the halocline

420 (related to the CDW) in the northern part of the study area in 2017. Contrary, thermocline and halocline were clearly separated in the southern part of the study area in 2015. The thermocline acts as physical barrier, which impedes vertical mixing and DO exchange with upper layers. Primary production in the CDW and related DO consumption in the near-bottom layers (Wang et al., 2017, 2016) cause DO decline. Zhu et al (2016) found that the area of DO concentration <3.0 mg l^{-1} relatively well fits with the region of the pycnocline strength > 2.0 kg m^{-}

425 ^{3}.

We have already outlined the main difference in the wind forcing behind formation of the hypoxia in the southern and northern parts of our study area. The one in the north develops under the conditions of summer monsoon. Intense hypoxia can start from very shallow depths (at 5 m) in the northern area (Fig. 5) and it can develop very fast under favorable conditions (Guo et al., 2019). On the other hand, hypoxia can decay easily due to wind stirring

430 or downwelling as we observed at N15 section in 2015. Thus, hypoxia in the northern part can be very pronounced, but disappears fast if forcing changes (Ni et al., 2016).

Hypoxia in the southern part of the study area was not so pronounced but quite stable as noted already by Zhu et al. (2011). Continuous decline of the DO from March to October in the southern part was well demonstrated by monthly measurements by Li et al. (2018). We suggest three main reasons for this. First, favorable wind conditions

435 for the southward transport are not that frequent in summer. Secondly, the mixture of CDW with ambient ocean

water promotes organic matter settling and nutrients consumption on the way to south, so less detritus sinks to the bottom layer and DO consumption is lower in the southern part comparing to the northern counterpart. Third, the area in the south is deeper and wind mixing does not destroy the thermocline. In short, the first two reasons account for a lighter hypoxia and the third for a long lasting hypoxia in the southern part.

440   We have demonstrated that DO conditions off the Changjiang Estuary are sensible to wind forcing. We extracted the wind climate projection data until 2099 from the Earth System model IPSL-CM5A-MR, but significant changes in the summer monsoon are not foreseen. Thus, future changes in the hypoxia off the Changjiang Estuary could be rather related to the increase in sea surface temperature and consequent extension of the stratified period, and to the intensification of eutrophication.

445

Conclusions

450   Two physical conditions in the water column must be present for the existence of hypoxia in the near-bottom layer off the Changjiang Estuary: thermocline and CDW. We found strong correlation between the vertical locations of oxycline (AOU isoline of 2 mg l⁻¹) and thermocline (isotherm 24.5 C°). Both clines (isolayers) revealed pronounced inclination, being at 50-60 m depth in the southeastern part and near the sea surface in the northern side of the study area.

455   Two very different stratification and DO distributions were registered in the area off the Changjiang Estuary in summers 2015 and 2017. Summer monsoon (wind from south) prevailed and Chinese Coastal Current was altered or even reversed in 2017. The CDW spread mainly to the northeast and east and caused pronounced hypoxic zone in the northern part of the study area. Hypoxic water occupied there most of the water column, as below the CDW at 5 - 8 m depth strong DO depletion revealed. Another low DO zone, connected to the low saline surface water and upwelled subsurface water, occurred in the southern part of the study area in 2017. According to the long-term wind statistics, this is the prevailing stratification and hypoxia pattern in the area during summers.

460   Northerly winds caused intensification of the Chinese Coastal Current and southward transport of the CDW before the survey in 2015. Northern part of the study area was well ventilated, but low DO zone revealed in the southern part. Such a situation occurs if summer monsoon is weaker than long-term average.

465   The two distribution patterns developed by southerly and northerly wind were confirmed by remotely sensed sea surface salinity fields and by circulation simulation. Wind forcing and river runoff are likely main contributors of inter-annual variations determining the size and location of low DO areas. Wind is the main driver of the annual cycle of the lateral DO minimum location. The minimum is located more likely in the northern part in July-August during summer monsoon and in the southern part during rest of the stratified period.

470

475

Code availability. Scripts to analyze the results are available upon request. Please contact TL.

Author contributions. TL lead the analyzes of the data and writing of the manuscript with contributions of DF and YW. DF was responsible to arrange oceanographic cruises.

480

Competing interests. We declare that no competing interests are present.

Acknowledgments. This research was funded by the National Natural Science Foundation of China (41776052), Qingdao National Laboratory for Marine Science and Technology (MGQNLM-TD201802), and the Research

485 Fund of State Key Laboratory of Marine Geology at Tongji University (MG20190104).

River data was downloaded from Bulletin of River Sediment in China provided by Ministry of Water Resources of the People's Republic of China (MWR). Website: http://www.mwr.gov.cn/sj/tjgb/zghlnsgb/ (visited 7th September 2019). We thank Yue Zhang for the gathering the CTD data in 2015 and Junbiao Tu for providing the mooring data. We would like to thank our colleagues who helped us in performing measurements. We thank Jaan

490 Laanemets for his comments on the manuscript.

References

495 Altieri, A. H. and Gedan, K. B.: Climate change and dead zones, Glob. Chang. Biol., 21(4), 1395–1406, doi:10.1111/gcb.12754, 2015.

Bailey, K., Steinberg, C., Davies, C., Galibert, G., Hidas, M., McManus, M. A., Murphy, T., Newton, J., Roughan, M. and Schaeffer, A.: Coastal Mooring Observing Networks and Their Data Products: Recommendations for the Next Decade, Front. Mar. Sci., 6, 180, doi:10.3389/fmars.2019.00180, 2019.

500 Beardsley, R. C., Limeburner, R., Yu, H. and Cannon, G. A.: Discharge of the Changjiang (Yangtze River) into the East China Sea, Cont. Shelf Res., 4(1–2), 57–76, doi:10.1016/0278-4343(85)90022-6, 1985.

Chen, J., Pan, D., Liu, M., Mao, Z., Zhu, Q., Chen, N., Zhang, X. and Tao, B.: Relationships Between Long-Term Trend of Satellite-Derived Chlorophyll-a and Hypoxia Off the Changjiang Estuary, Estuaries and Coasts, 40(4), 1055–1065, doi:10.1007/s12237-016-0203-0, 2017.

505 Chen, Y.-L. L., Chen, H.-Y., Gong, G.-C., Lin, Y.-H., Jan, S. and Takahashi, M.: Phytoplankton production during a summer coastal upwelling in the East China Sea, Cont. Shelf Res., 24, 1321–1338, doi:10.1016/j.csr.2004.04.002, 2004.

Chu, P., Yuchun, C. and Kuninaka, A.: Seasonal variability of the Yellow Sea/East China Sea surface fluxes and thermohaline structure, Adv. Atmos. Sci., 22(1), 1–20, doi:10.1007/BF02930865, 2005.

510 Conley, D. J., Björck, S., Bonsdorff, E., Carstensen, J., Destouni, G., Gustafsson, B. G., Hietanen, S., Kortekaas, M., Kuosa, H., Markus Meier, H. E., Müller-Karulis, B., Nordberg, K., Norkko, A., Nürnberg, G., Pitkänen, H., Rabalais, N. N., Rosenberg, R., Savchuk, O. P., Slomp, C. P., Voss, M., Wulff, F. and Zillén, L.: Hypoxia-

Related Processes in the Baltic Sea, Environ. Sci. Technol., 43(10), 3412–3420, doi:10.1021/es802762a, 2009.

Csanady, G. T.: Circulation in the Coastal Ocean, Adv. Geophys., 23, 101–183, doi:10.1016/S0065-2687(08)60331-3, 1981.

515

Cui, Y., Wu, J., Ren, J. and Xu, J.: Physical dynamics structures and oxygen budget of summer hypoxia in the Pearl River Estuary, Limnol. Oceanogr., 64(1), 131–148, doi:10.1002/lno.11025, 2019.

Diaz, R. J. and Rosenberg, R.: Spreading dead zones and consequences for marine ecosystems., Science, 321(5891), 926–9, doi:10.1126/science.1156401, 2008.

520 Fofonoff, N. P. and Millard Jr, R. C.: Algorithms for the computation of fundamental properties of seawater., UNESCO. [online] Available from: https://www.oceanbestpractices.net/handle/11329/109 (Accessed 30 August 2019), 1983.

Fong, D. A. and Geyer, W. R.: The Alongshore Transport of Freshwater in a Surface-Trapped River Plume*, J. Phys. Oceanogr., 32(3), 957–972, doi:10.1175/1520-0485(2002)032<0957:TATOFI>2.0.CO;2, 2002.

525 Guo, Y., Rong, Z., Li, B., Xu, Z., Li, P. and Li, X.: Physical processes causing the formation of hypoxia off the Changjiang estuary after Typhoon Chan-hom, 2015, J. Oceanol. Limnol., 37(1), 1–17, doi:10.1007/s00343-019-7336-5, 2019.

Hu, J. and Wang, X. H.: Progress on upwelling studies in the China seas, Rev. Geophys., 54(3), 653–673, doi:10.1002/2015RG000505, 2016.

530 Hung, C.-C., Chung, C.-C., Gong, G.-C., Jan, S., Tsai, Y., Chen, K.-S., Chou, W. C., Lee, M.-A., Chang, Y., Chen, M.-H., Yang, W.-R., Tseng, C.-J. and Gawarkiewicz, G.: Nutrient supply in the Southern East China Sea after Typhoon Morakot, J. Mar. Res., 71(1), 133–149, doi:10.1357/002224013807343425, 2013.

Kang, Y., Pan, D., Bai, Y., He, X., Chen, X., Chen, C.-T. A. and Wang, D.: Areas of the global major river plumes, Acta Oceanol. Sin., 32(1), 79–88, doi:10.1007/s13131-013-0269-5, 2013.

535 Large, W. G. and Pond, S.: Open Ocean Momentum Flux Measurements in Moderate to Strong Winds, J. Phys. Oceanogr., 11(3), 324–336, doi:10.1175/1520-0485(1981)011<0324:OOMFMI>2.0.CO;2, 1981.

Lentz, S. J. and Helfrich, K. R.: Buoyant gravity currents along a sloping bottom in a rotating fluid, J. Fluid Mech, 464, 251–278, doi:10.1017/S0022112002008868, 2002.

Li, L., He, Z., Xia, Y. and Dou, X.: Dynamics of sediment transport and stratification in Changjiang River Estuary, China, Estuar. Coast. Shelf Sci., 213, 1–17, doi:10.1016/J.ECSS.2018.08.002, 2018a.

540

Li, M. and Chen, Z.: An Assessment of Saltwater Intrusion in the Changjiang (Yangtze) River Estuary, China, Coasts and Estuaries, 31–43, doi:10.1016/B978-0-12-814003-1.00002-2, 2019.

Li, M. and Rong, Z.: Effects of tides on freshwater and volume transports in the Changjiang River plume, J. Geophys. Res, 117, 6027, doi:10.1029/2011JC007716, 2012.

545 Li, Z., Song, S., Li, C. and Yu, Z.: The sinking of the phytoplankton community and its contribution to seasonal hypoxia in the Changjiang (Yangtze River) estuary and its adjacent waters, Estuar. Coast. Shelf Sci., 208, 170–179, doi:10.1016/J.ECSS.2018.05.007, 2018b.

Liblik, T., Karstensen, J., Testor, P., Alenius, P., Hayes, D., Ruiz, S., Heywood, K. J., Pouliquen, S., Mortier, L. and Mauri, E.: Potential for an underwater glider component as part of the Global Ocean Observing System, 550 Methods Oceanogr., 17, 50–82, doi:10.1016/j.mio.2016.05.001, 2016.

Lie, H.-J. and Cho, C.-H.: Recent advances in understanding the circulation and hydrography of the East China Sea, Fish. Oceanogr., 11(6), 318–328, doi:10.1046/j.1365-2419.2002.00215.x, 2002.

Lie, H.-J. and Cho, C.-H.: Seasonal circulation patterns of the Yellow and East China Seas derived from satellite-tracked drifter trajectories and hydrographic observations, Prog. Oceanogr., 146, 121–141, 555 doi:10.1016/J.POCEAN.2016.06.004, 2016.

Lips, U., Kikas, V., Liblik, T. and Lips, I.: Multi-sensor in situ observations to resolve the sub-mesoscale features in the stratified Gulf of Finland, Baltic Sea, Ocean Sci., 12(3), 715–732, doi:10.5194/os-12-715-2016, 2016.

560   Liu, Z. and Gan, J.: Modeling Study of Variable Upwelling Circulation in the East China Sea: Response to a Coastal Promontory, J. Phys. Oceanogr., 44(4), 1078–1094, doi:10.1175/JPO-D-13-0170.1, 2014.

Meissner, T., Wentz, F. J. and Manaster, A.: Remote Sensing Systems SMAP Ocean Surface Salinities [Level 2C, Level 3 Running 8-day, Level 3 Monthly], Version 3.0 validated release. Remote Sensing Systems, Santa Rosa, CA, USA., , doi:10.5067/SSSSS-TTTTT, 2018.

565   Moon, J.-H., Kim, T., Son, Y. B., Hong, J.-S., Lee, J.-H., Chang, P.-H. and Kim, S.-K.: Contribution of low-salinity water to sea surface warming of the East China Sea in the summer of 2016, Prog. Oceanogr., 175, 68–80, doi:10.1016/j.pocean.2019.03.012, 2019.

Ni, X., Huang, D., Zeng, D., Zhang, T., Li, H. and Chen, J.: The impact of wind mixing on the variation of bottom dissolved oxygen off the Changjiang Estuary during summer, J. Mar. Syst., 154, 122–130, doi:10.1016/j.jmarsys.2014.11.010, 2016.

570   Ning, X., Lin, C., Su, J., Liu, C., Hao, Q. and Le, F.: Long-term changes of dissolved oxygen, hypoxia, and the responses of the ecosystems in the East China Sea from 1975 to 1995, J. Oceanogr., 67(1), 59–75, doi:10.1007/s10872-011-0006-7, 2011.

Obenour, D. R., Scavia, D., Rabalais, N. N., Turner, R. E. and Michalak, A. M.: Retrospective Analysis of Midsummer Hypoxic Area and Volume in the Northern Gulf of Mexico, 1985–2011, Environ. Sci. Technol., 575   47(17), 9808–9815, doi:10.1021/es400983g, 2013.

Peng, L., Benwei, S., Yaping, W., Weihua, Q., Yangang, L. and Jian, C.: Analysis of the characteristics of offshore currents in the Changjiang (Yangtze River) estuarine waters based on buoy observations, Acta Ocean. Sin., 36(4), 13–20, doi:10.1007/s13131, 2017.

Ren, F., Fan, D., Wu, Y. and Zhao, Q.: The evolution of hypoxia off the Changjiang Estuary in the last 580   3000 years: Evidence from benthic foraminifera and elemental geochemistry, Mar. Geol., 417, 106039, doi:10.1016/J.MARGEO.2019.106039, 2019.

Rudnick, D. L.: Ocean Research Enabled by Underwater Gliders, Ann. Rev. Mar. Sci., 8(1), 519–541, doi:10.1146/annurev-marine-122414-033913, 2016.

Sun, H., Yang, Q., Zhao, W., Liang, X. and Tian, J.: Temporal variability of diapycnal mixing in the northern 585   South China Sea, J. Geophys. Res. Ocean., 121(12), 8840–8848, doi:10.1002/2016JC012044, 2016.

Testa, J. M. and Kemp, W. M.: Spatial and Temporal Patterns of Winter–Spring Oxygen Depletion in Chesapeake Bay Bottom Water, Estuaries and Coasts, 37(6), 1432–1448, doi:10.1007/s12237-014-9775-8, 2014.

Tseng, Y.-F., Lin, J., Dai, M. and Kao, S.-J.: Joint effect of freshwater plume and coastal upwelling on phytoplankton growth off the Changjiang River, Biogeosciences, 11(2), 409–423, doi:10.5194/bg-11-409-2014, 590   2014.

Vaquer-Sunyer, R. and Duarte, C. M.: Thresholds of hypoxia for marine biodiversity., Proc. Natl. Acad. Sci. U. S. A., 105(40), 15452–7, doi:10.1073/pnas.0803833105, 2008.

Venkatesan, R., Lix, J. K., Phanindra Reddy, A., Arul Muthiah, M. and Atmanand, M. A.: Two decades of operating the Indian moored buoy network: significance and impact, J. Oper. Oceanogr., 9(1), 45–54, 595   doi:10.1080/1755876X.2016.1182792, 2016.

Wang, B. and Wang, X.: Chemical hydrography of coastal upwelling in the East China Sea, Chinese J. Oceanol. Limnol., 25(1), 16–26, doi:10.1007/s00343-007-0016-x, 2007.

Wang, B., Wei, Q., Chen, J. and Xie, L.: Annual cycle of hypoxia off the Changjiang (Yangtze River) Estuary, Mar. Environ. Res., 77, 1–5, doi:10.1016/j.marenvres.2011.12.007, 2012.

600   Wang, B., Chen, J., Jin, H., Li, H., Huang, D. and Cai, W.-J.: Diatom bloom-derived bottom water hypoxia off the Changjiang estuary, with and without typhoon influence, Limnol. Oceanogr., 62(4), 1552–1569, doi:10.1002/lno.10517, 2017.

Wang, H., Dai, M., Liu, J., Kao, S.-J., Zhang, C., Cai, W.-J., Wang, G., Qian, W., Zhao, M. and Sun, Z.: Eutrophication-Driven Hypoxia in the East China Sea off the Changjiang Estuary, Environ. Sci. Technol., 50(5), 605   2255–2263, doi:10.1021/acs.est.5b06211, 2016.

Wei, Q., Wang, B., Yu, Z., Chen, J. and Xue, L.: Mechanisms leading to the frequent occurrences of hypoxia

and a preliminary analysis of the associated acidification off the Changjiang estuary in summer, Sci. China Earth Sci., 60(2), 360–381, doi:10.1007/s11430-015-5542-8, 2017a.

Wei, Q., Yu, Z., Wang, B., Wu, H., Sun, J., Zhang, X., Fu, M., Xia, C. and Wang, H.: Offshore detachment of the Changjiang River plume and its ecological impacts in summer, J. Oceanogr., 73(3), 277–294, doi:10.1007/s10872-016-0402-0, 2017b.

Weiss, R. F.: The solubility of nitrogen, oxygen and argon in water and seawater, Deep Sea Res. Oceanogr. Abstr., 17(4), 721–735, doi:10.1016/0011-7471(70)90037-9, 1970.

Wu, H., Deng, B., Yuan, R., Hu, J., Gu, J., Shen, F., Zhu, J., Zhang, J., Wu, H., Deng, B., Yuan, R., Hu, J., Gu, J., Shen, F., Zhu, J. and Zhang, J.: Detiding Measurement on Transport of the Changjiang-Derived Buoyant Coastal Current, J. Phys. Oceanogr., 43(11), 2388–2399, doi:10.1175/JPO-D-12-0158.1, 2013.

Wu, Y., Fan, D., Wang, D. and Yin, P.: Increasing hypoxia in the Changjiang Estuary during the last three decades deciphered from sedimentary redox-sensitive elements, Mar. Geol., 106044, doi:10.1016/J.MARGEO.2019.106044, 2019.

Xu, Q., Zhang, S., Cheng, Y. and Zuo, J.: Interannual Feature of Summer Upwelling around the Zhoushan Islands in the East China Sea, J. Coast. Res., 331, 125–134, doi:10.2112/JCOASTRES-D-15-00197.1, 2017.

Xu, Z., Ma, J., Wang, H., Hu, Y., Yang, G., Deng, W., Xu, Z., Ma, J., Wang, H., Hu, Y., Yang, G. and Deng, W.: River Discharge and Saltwater Intrusion Level Study of Yangtze River Estuary, China, Water, 10(6), 683, doi:10.3390/w10060683, 2018.

Xuan, J.-L., Huang, D., Zhou, F., Zhu, X.-H. and Fan, X.: The role of wind on the detachment of low salinity water in the Changjiang Estuary in summer, J. Geophys. Res. Ocean., 117(C10), n/a-n/a, doi:10.1029/2012JC008121, 2012.

Yang, L., Chen, Z., Sun, Z. and Hu, J.: Sectional characteristics of temperature, salinity and density off the central Zhejiang coast in the spring of 2016, Acta Oceanol. Sin., 38(4), 175–182, doi:10.1007/s13131-019-1421-7, 2019.

Ye, W., Zhang, G., Zhu, Z., Han, Y., Wang, L. and Sun, M.: Methane distribution and sea-to-air flux in the East China Sea during the summer of 2013: Impact of hypoxia, Deep Sea Res. Part II Top. Stud. Oceanogr., 124, 74–83, doi:10.1016/J.DSR2.2015.01.008, 2016.

Zhang, L., Liu, Z., Zhang, J., Hong, G. H., Park, Y. and Zhang, H. F.: Reevaluation of mixing among multiple water masses in the shelf: An example from the East China Sea, Cont. Shelf Res., 27(15), 1969–1979, doi:10.1016/J.CSR.2007.04.002, 2007.

Zhang, W., Wu, H. and Zhu, Z.: Transient Hypoxia Extent Off Changjiang River Estuary due to Mobile Changjiang River Plume, J. Geophys. Res. Ocean., 123(12), 9196–9211, doi:10.1029/2018JC014596, 2018.

Zhou, Z., Yu, R., Sun, C., Feng, M. and Zhou, M.: Impacts of Changjiang River Discharge and Kuroshio Intrusion on the Diatom and Dinoflagellate Blooms in the East China Sea, J. Geophys. Res. Ocean., 124(7), 2019JC015158, doi:10.1029/2019JC015158, 2019.

Zhu, J., Zhu, Z., Lin, J., Wu, H. and Zhang, J.: Distribution of hypoxia and pycnocline off the Changjiang Estuary, China, J. Mar. Syst., 154, 28–40, doi:10.1016/j.jmarsys.2015.05.002, 2016.

Zhu, Z.-Y., Zhang, J., Wu, Y., Zhang, Y.-Y., Lin, J. and Liu, S.-M.: Hypoxia off the Changjiang (Yangtze River) Estuary: Oxygen depletion and organic matter decomposition, Mar. Chem., 125(1–4), 108–116, doi:10.1016/J.MARCHEM.2011.03.005, 2011.

Zuo, J., Song, J., Yuan, H., Li, X., Li, N. and Duan, L.: Impact of Kuroshio on the dissolved oxygen in the East China Sea region, J. Oceanol. Limnol., 37(2), 513–524, doi:10.1007/s00343-019-7389-5, 2019.
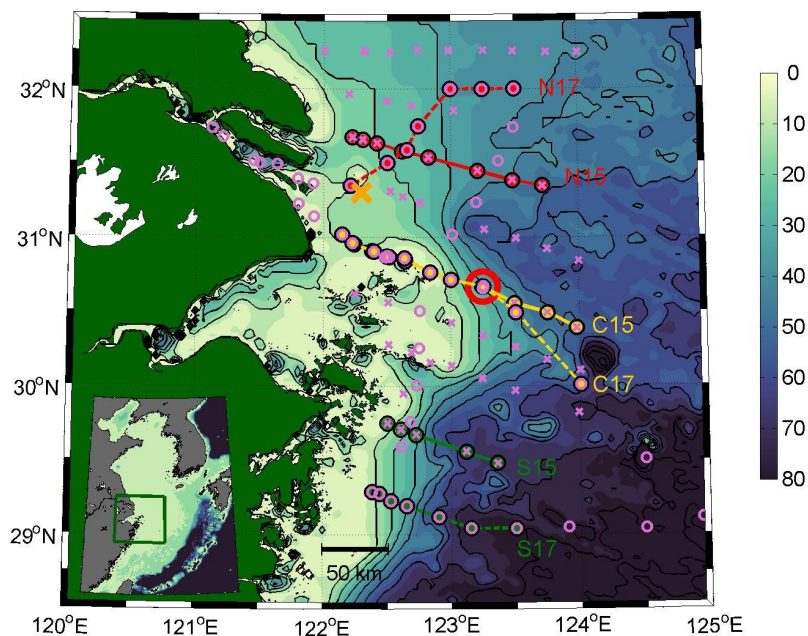
650

Figure 1. Map of the study area off the Changjiang Estuary. Purple crosses represent CTD cast stations conducted on 27 August – 5 September in 2015 and purple circles show CTD cast stations on 24 - 29 July in 2017. Red lines represent northerly sections (N15 in 2015 and N17 in 2017), yellow lines central sections (C15 in 2015 and C17 in 2017), and green lines southern sections (S15 in 2015 and S17 in 2017). Larger red
655 **circle represents the mooring M1 location. Orange larger cross shows the location, where wind data were gathered. Color scale shows depth (m) of the study area. The inlay shows the study area in the East China Sea.**
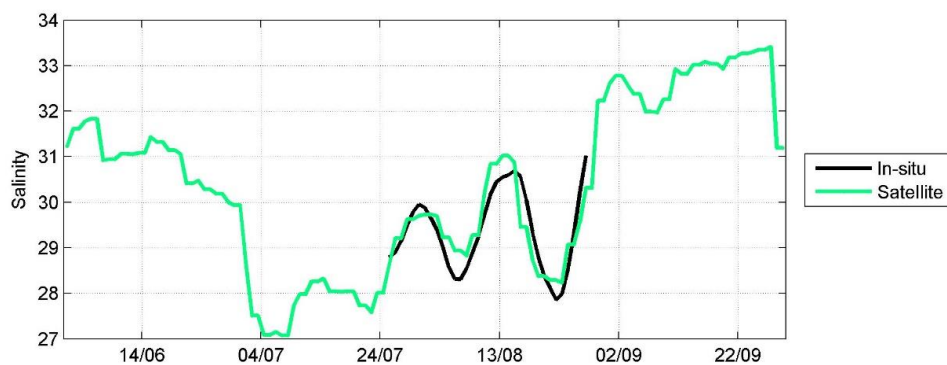
Figure 2. Time-series of in-situ and remotely sensed 8-day running mean salinity at the M1 location in 2017.

660
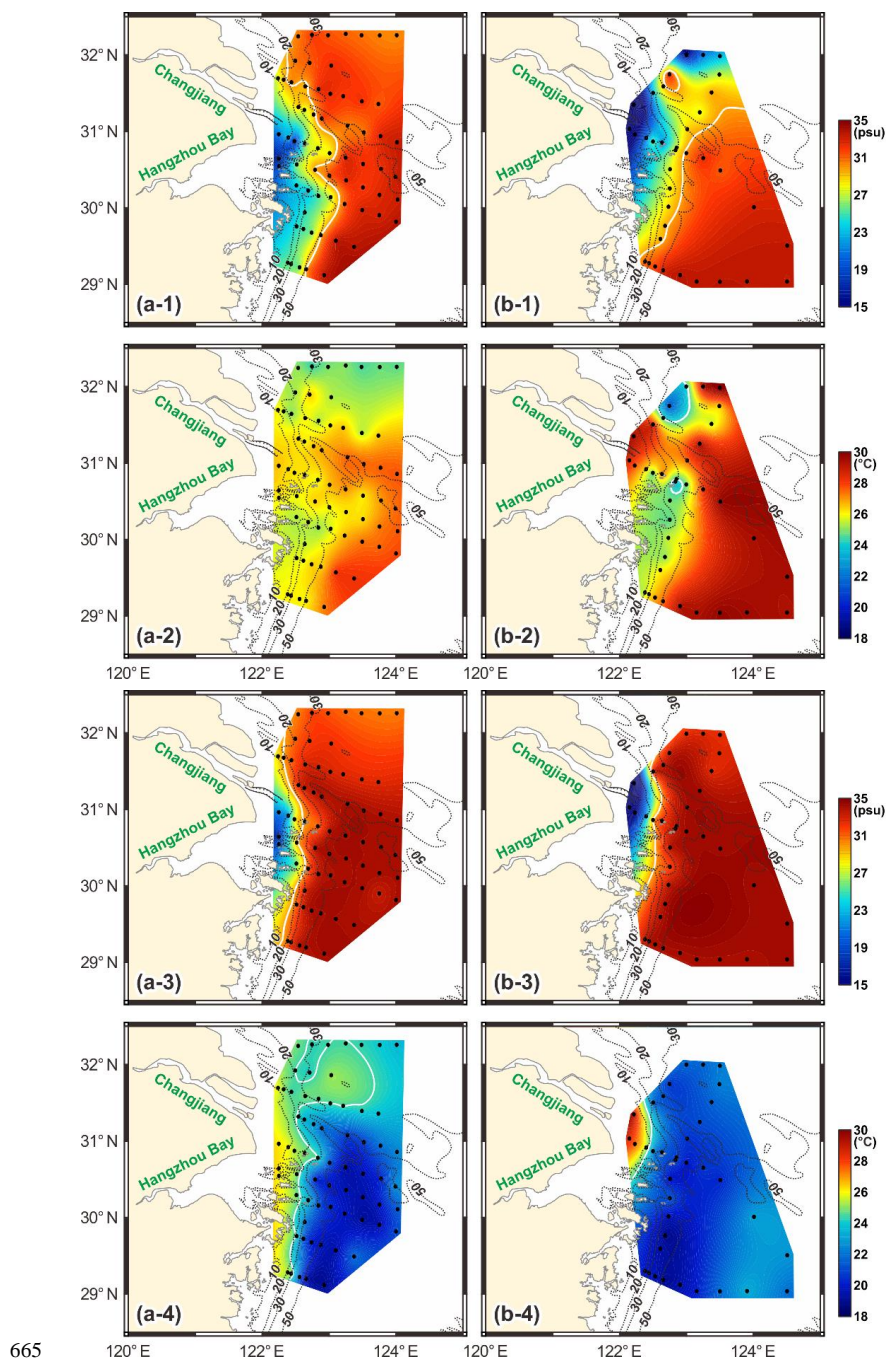
Figure 3. Maps of surface salinity (a-1 and b-1), surface temperature (a-2 and b-2), near-bottom salinity (a-3, b-3) and near-bottom temperature (a-4, b-4) from the surveys in 2015 (left panel) and 2017 (right panel). 24.5 °C and 31 psu isolines are shown as white lines.
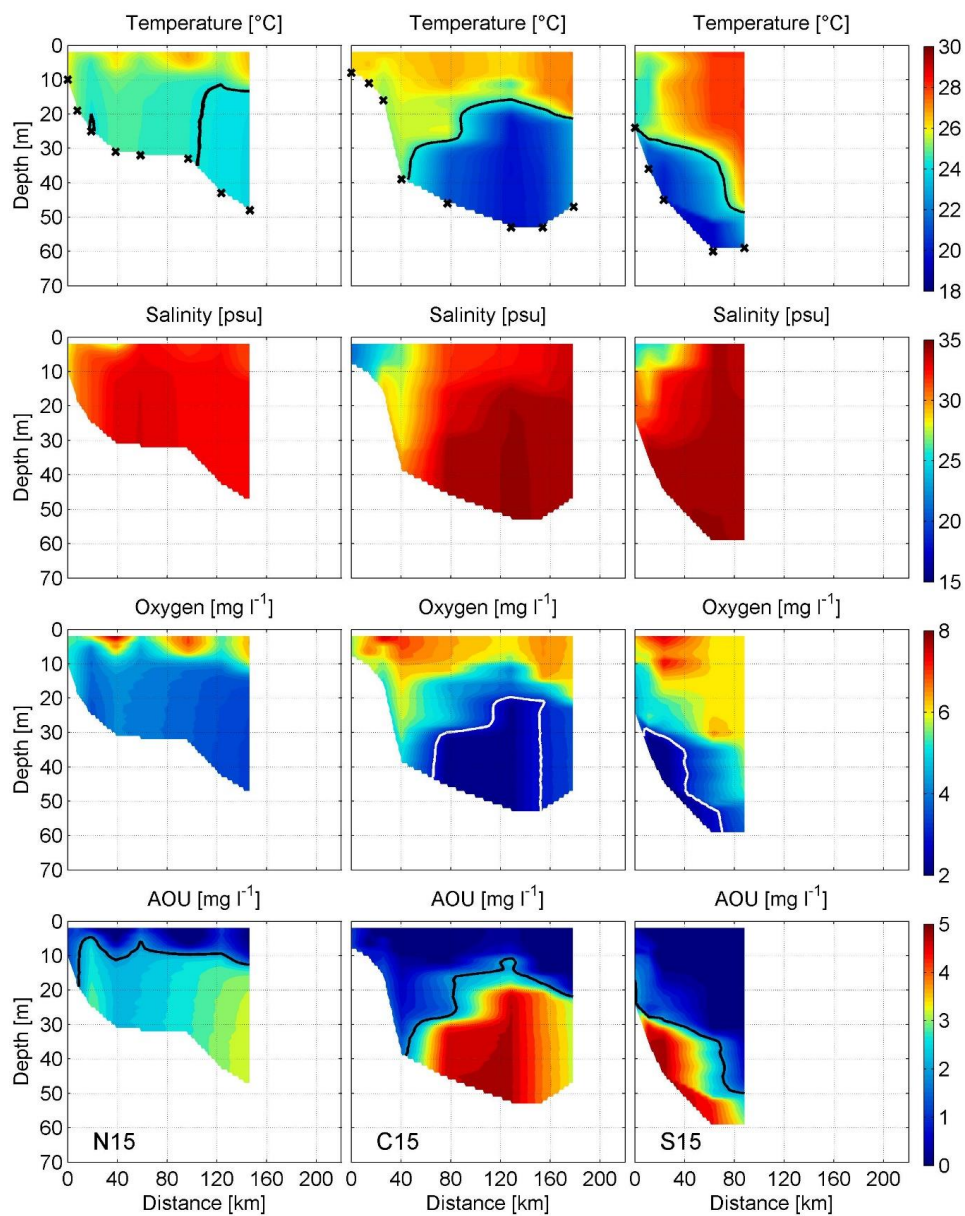
670

Fig. 4. Vertical distributions of temperature, salinity, density, DO concentration, and Apparent Oxygen Utilization (AOU) along sections N15, C15, and S15 in 2015 (Fig. 1). Temperature isoline 24.5 °C and AOU isoline 2 mg l⁻¹ are shown with solid black line. Hypoxia border (3.0 mg l⁻¹) is shown with solid white line. Values on the *x*-axis indicate the distance from the westernmost point of a section (Fig. 1).
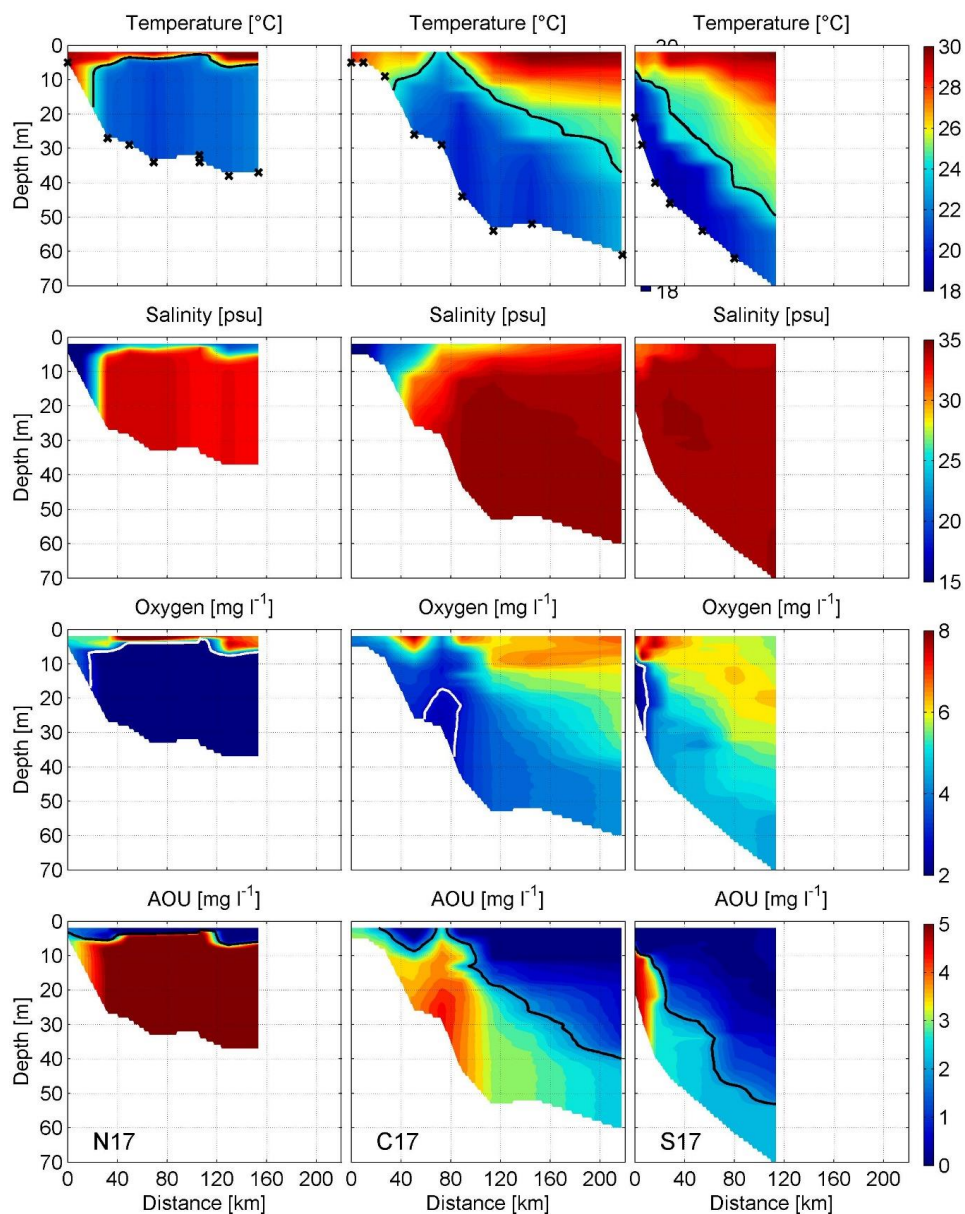
675

Fig. 5. Vertical distributions of temperature, salinity, density, DO concentration and AOU along sections N17, C17, S17 in 2017 (Fig. 1). Temperature isoline 24.5 °C and AOU isoline 2 mg l^{-1} (upper panels) are shown with solid black line. Hypoxia border (3.0 mg l^{-1}) is shown with solid white line. Values on the *x*-axis indicate the distance from the westernmost point of a section (Fig. 1).
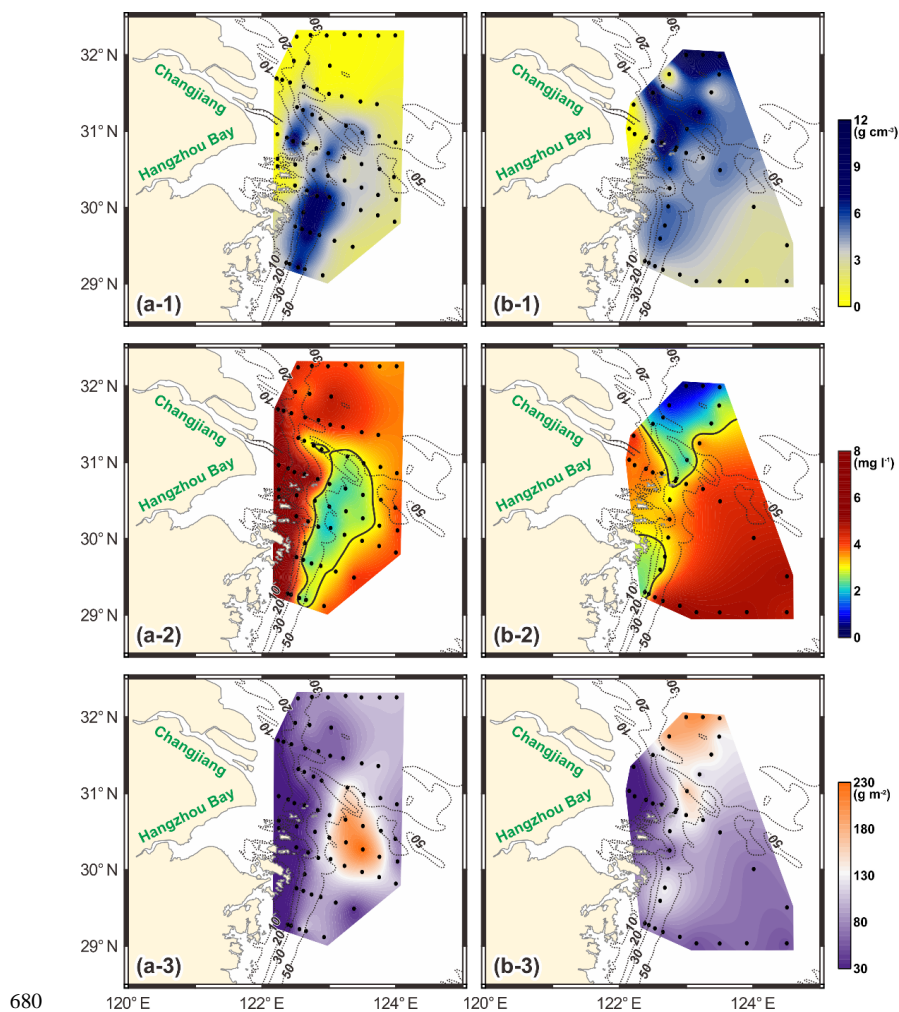
Fig 6. Maps of density difference between the near-bottom layer and surface layer (upper panel), near-bottom DO (mid-panel) and total AOU in the water column (lowest panel) in 2015 (left) and 2017 (right). Only positive values of AOU were used in the vertical integration of the AOU profile.
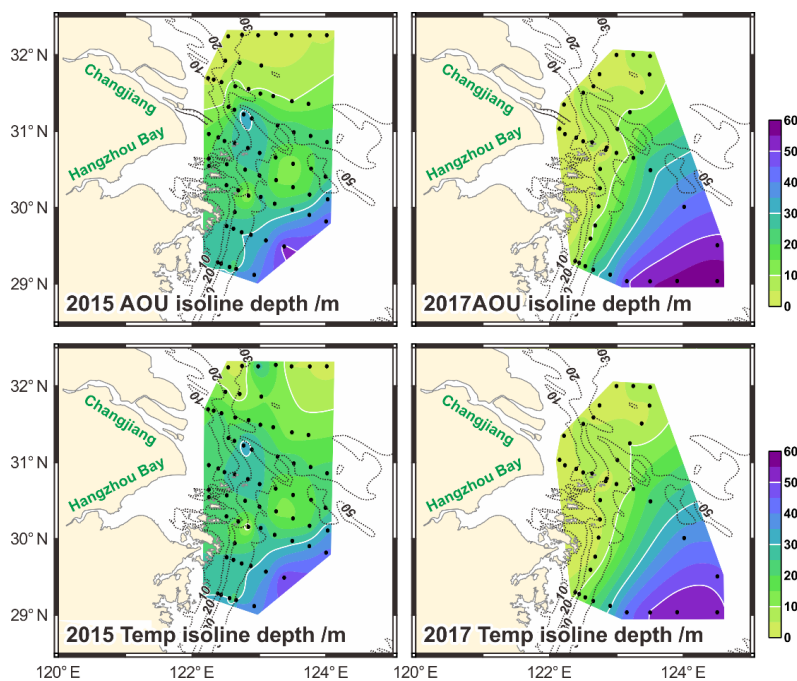
Fig. 7. Maps of AOU isoline 2 mg l⁻¹ depth (upper panels) and temperature isoline 24.5 °C depth (lower panels) in 2015 (left panels) and in 2017 (right panels).

685
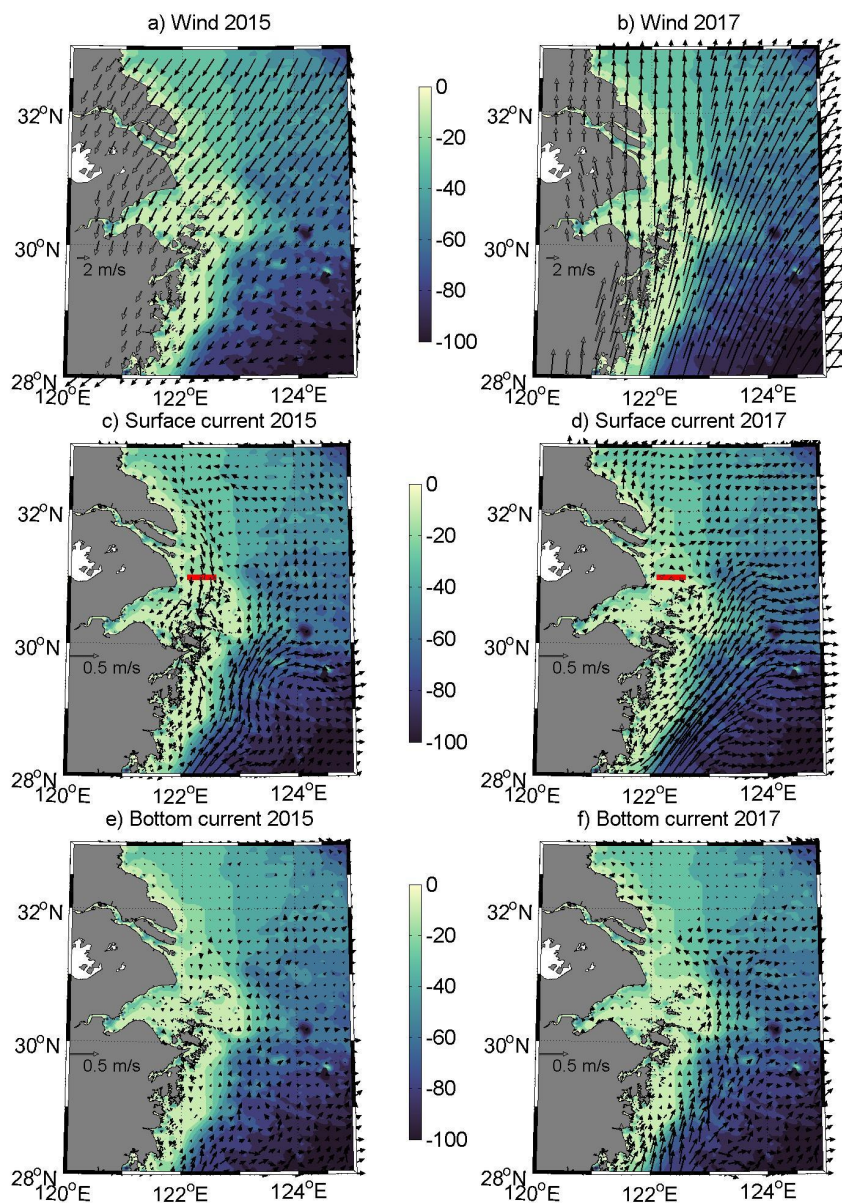
Figure 8. Maps of mean wind (upper panels), simulated surface current (middle panels) and bottom current (bottom panels) 7 days prior to the CTD surveys. Bottom bathymetry is shown as a background. Red lines show the section S1, where current time-series were calculated. Every fourth current vector is shown only. Persistent current in the southeastern side is the Taiwan Warm Current.

690
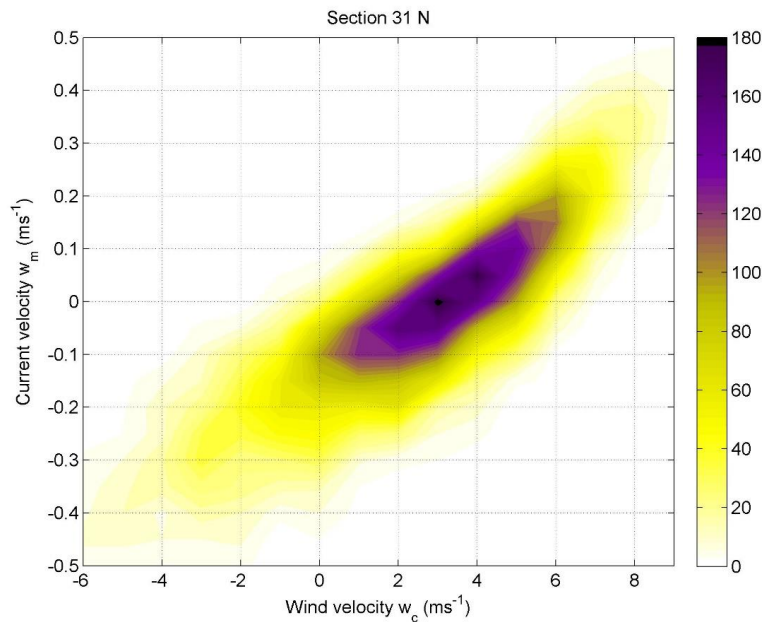
Figure 9. Relation of daily mean SE-NW wind velocity component w_c (positive towards NW) and meridional current velocity component v_m (positive northward) in the section at 31° (section S1 in Fig. 8) in 1993-2018. Wind speed steps of 1 m s^{-1} for wind velocity component and 0.05 m s^{-1} for current velocity component were used to calculate histogram. Color scale shows the co-occurrence (number of cases) of respective wind velocity and current velocity component combinations.

695
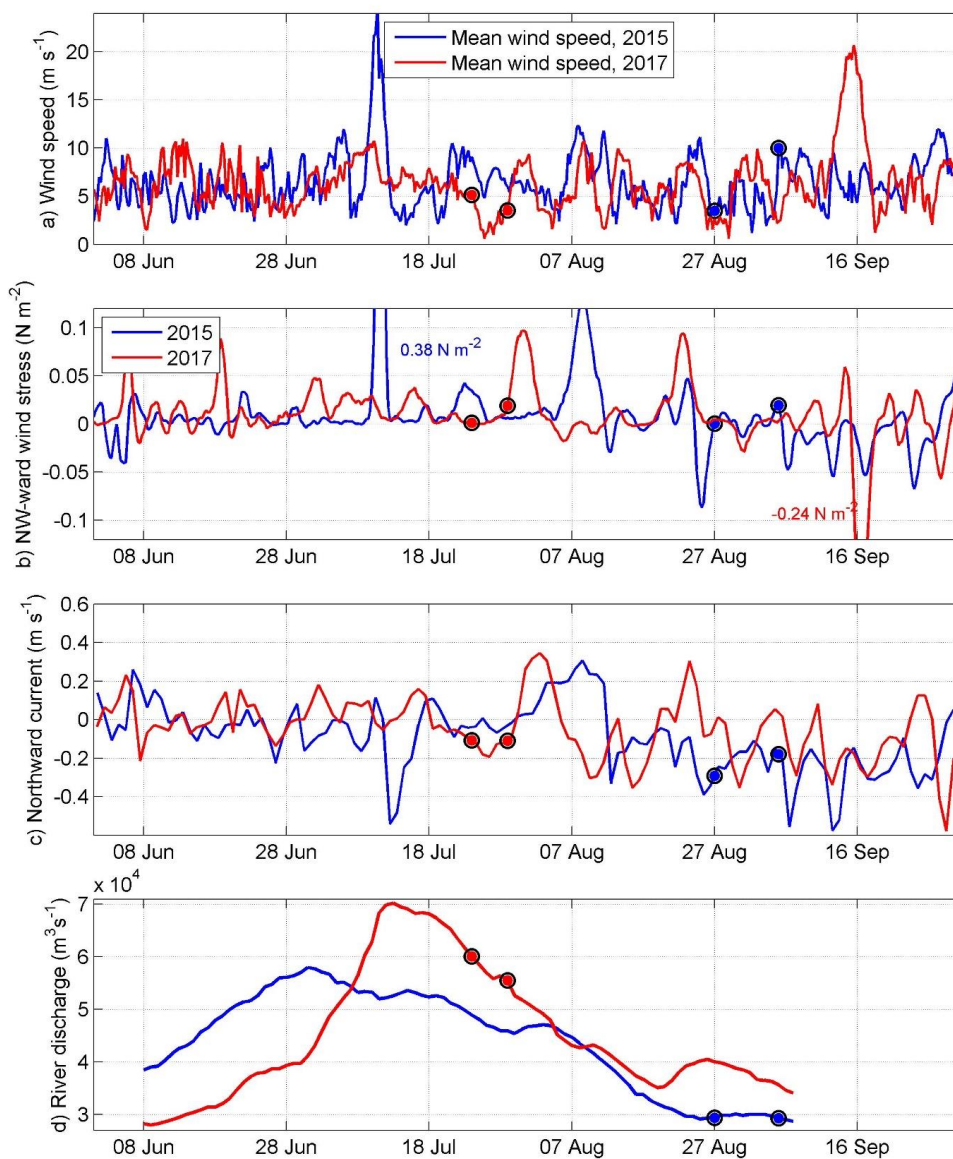
Figure 10. Time-series of wind, current, and river discharge. Mean wind speed (6-hours) (a), 1-day running mean SE-NW wind stress τ_c (positive towards NW; N m^{-2}) (b), daily mean meridional current velocity component v_m (positive northward) at section S1 (c), and daily Changjiang river discharge at Datong station shifted by 7 days to represent flow in the river mouth (d). Blue and red dots represent start and end of the CTD surveys, respectively in 2015 and 2017.

700
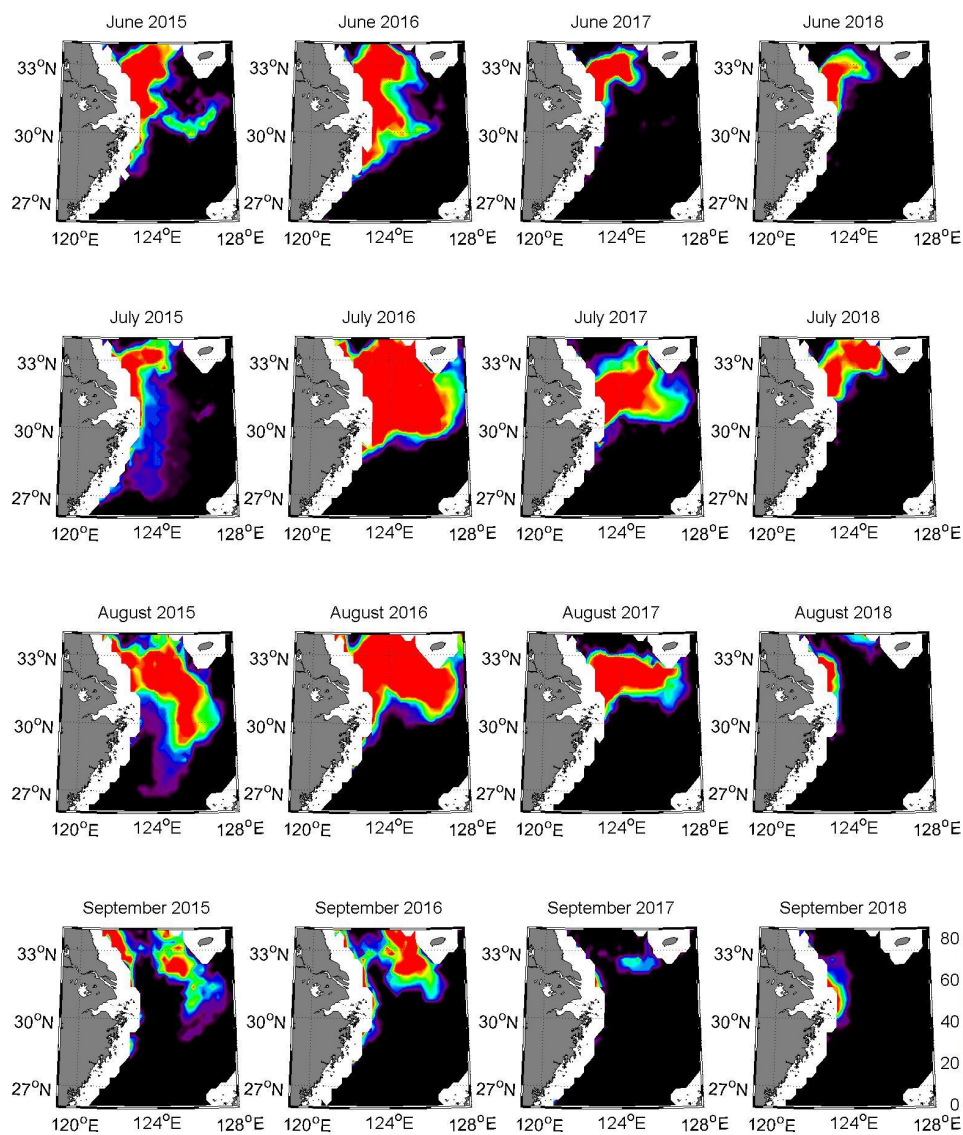
705 **Figure 11. Maps of monthly occurrence (%) of (remotely sensed) salinity < 30 g kg⁻¹ from June to September, 2015-2018.**
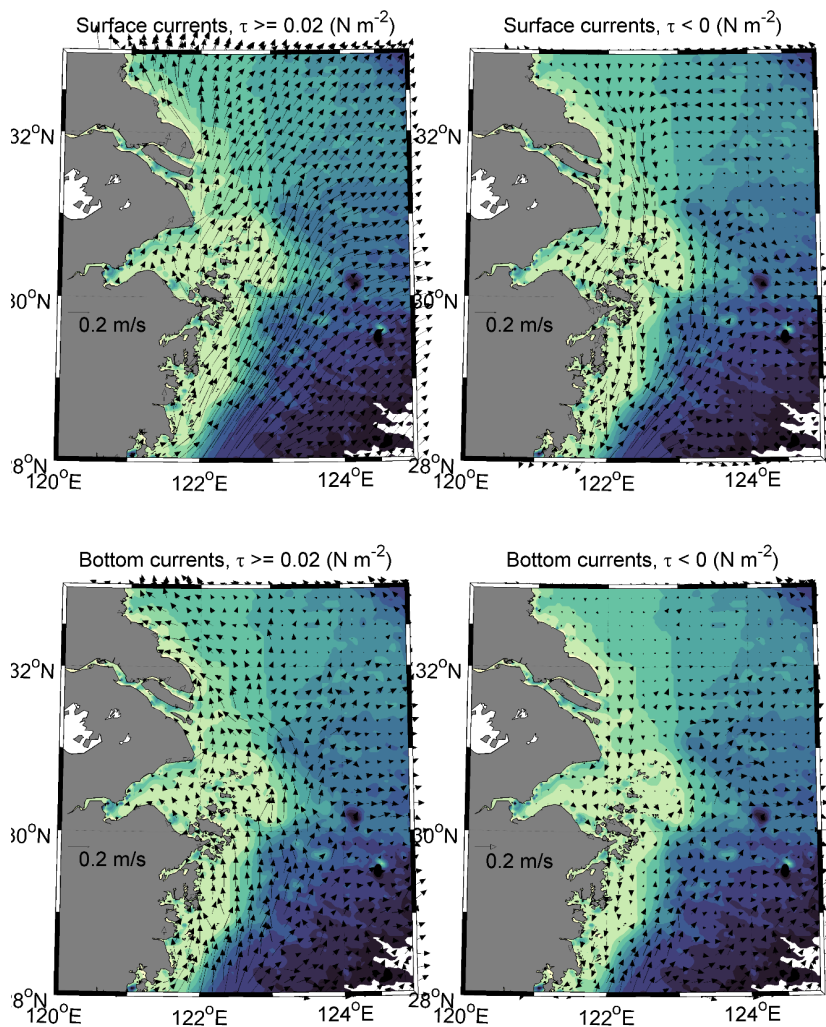
Figure 12. Maps of surface (upper panels) and near-bottom (lower panels) currents in the cases of wind stress component $\tau_c \geq 0.02$ N m^{-2} (left panels) and $\tau_c < 0$ N m^{-2} (right panels) in 1993-2018. Every fourth current vector is shown.
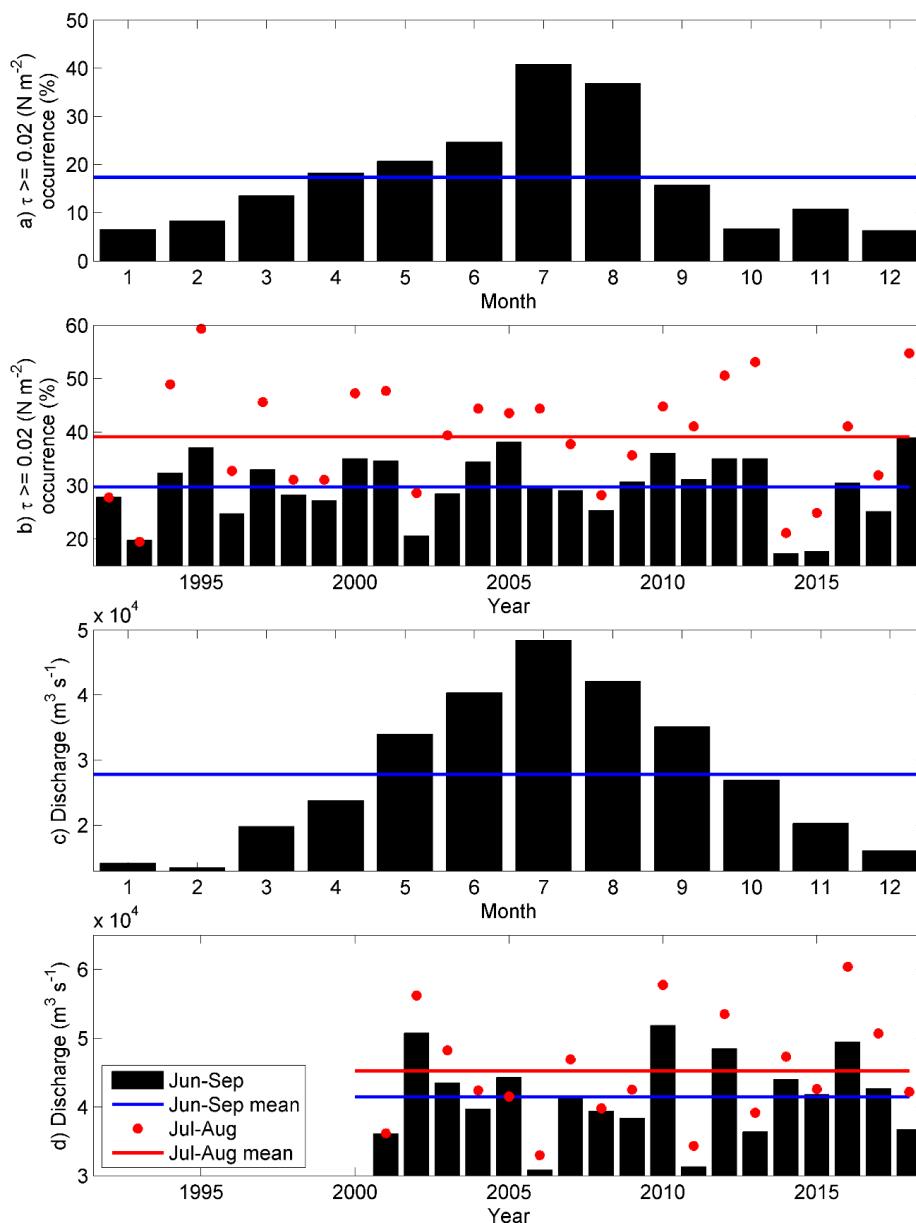
Figure 13. Annual cycle (a, c) and inter-annual variability (b, d) of wind stress component (1992-2018) $\tau_c \geq$ 0.02 N m^{-2} (a, b) and river discharge (c, d) (2001-2018). Blue line shows the overall mean in (a) and (c), and June-September long-term mean in (c) and (d). Red line shows the July-August long-term mean in (b) and (d).

720 **Table 1. Summary of general features observed in the study area in summers 2015 and 2017**

Summer 2015	Summer 2017
Southward transport of the CDW	East/northeastward transport of the CDW
Stronger stratification in the south	Stronger stratification in the north
Generally lower SST	Generally higher SST
No low DO concentration zone in the north	Strong and shallow hypoxic zone in the north
Bottom water warmer and fresher in the north	Bottom water colder and saltier in the north
Lower DO concentrations further offshore at sea depths >=30 m in the south	Lower DO concentrations in the coastal upwelling zone in the south